Electron-Phonon Interaction and Localization of Surface-State Carriers in a Metallic Monolayer

Iwao Matsuda,[*] Canhua Liu, Toru Hirahara, Masashi Ueno, Takehiro Tanikawa, Taizo Kanagawa, Rei Hobara,
Shiro Yamazaki, and Shuji Hasegawa

Department of Physics, School of Science, The University of Tokyo, 7-3-1 Hongo, Bunkyo-ku, Tokyo 113-0033, Japan

Katsuyoshi Kobayashi

Department of Physics, Faculty of Science, Ochanomizu University, 2-1-1 Otsuka, Bunkyo-ku, Tokyo 112-8610, Japan
(Received 5 December 2006; published 4 October 2007)

Temperature-dependent electron transport in a metallic surface superstructure, $Si(111)\sqrt{3} \times \sqrt{3}$-Ag, was studied by a micro-four-point probe method and photoemission spectroscopy. The surface-state conductivity exhibits a sharp transition from metallic conduction to strong localization at ~ 150 K. The metallic regime is due to electron-phonon interaction while the localization seemingly originates from coherency of electron waves. Random potential variations, caused by Friedel oscillations of surface electrons around defects, likely induce strong carrier localization.

Electron transport phenomena through low-dimensional materials have been major topics in condensed matter physics [1]. The reduction of the dimensionality of electron systems induces various quantum transport properties that are specific to each dimension. For example, based on the scaling theory, electrons in one- and two-dimensions (1D, 2D) are always localized with an arbitrary amount of scatterers, in contrast with the case of three dimensions (3D) [2]. For the past decades, experimental research about localization have been vigorously performed mainly in the semiconductor-superlattice systems such as modulation doped AlGaAs/GaAs structures [1,2].

Recently, there has been growing interest in solid surfaces or surface superstructures as a new playground to study electron transports through 1D and 2D structures on atomic or nanometer scales [3,4]. This is mainly due to the recent development of the micro-four-point probe (MFPP) techniques, which enable surface conductivity measurements with high precision and reproducibility [5,6]. The main feature of a surface is that the thickness is only a monatomic layer, the smallest thickness of material, and it is much smaller than that of conventional semiconductor heterostructures that are submicron thick typically. Thus, it is of great interest to study transport phenomena in this new low-dimensional system.

In this Letter, we present surface transport experiments on a 2D metallic monolayer on a semiconductor surface. We chose a $Si(111)\sqrt{3} \times \sqrt{3}$-Ag surface superstructure as a sample. This surface possesses an isotropic 2D free-electron-like metallic surface-state band that is revealed by angle-resolved photoemission spectroscopy (ARPES) [7–9] as well as scanning tunneling microscopy or spectroscopy (STM/S) as electron standing waves around defects [10,11]. Through measuring temperature dependence of the surface conductivity by the MFPP method, the surface-state conductivity becomes large with decreasing temperature from room temperature (RT). The change is

described in terms of the surface electron-phonon (e-ph) interaction, which is quantitatively in accord with temperature-dependent ARPES results. Below ~ 150 K, the surface conductivity started to decrease by further cooling. Since the surface band structure remains metallic by cooling, we propose that such an insulating behavior corresponds to strong localization caused by random potentials due to Friedel oscillations induced around surface impurities and defects [10,11]. Density functional calculations with the jellium model demonstrate that the effect of Friedel oscillation on potential variation is negligible in typical 3D bulk metals, while it is significantly enhanced for the surface or the monatomic layer system.

Electrical conductivity was measured *in situ* by the MFPP method in a ultrahigh vacuum chamber, using our homemade independently driven four-tip STM prober [6] and temperature-controlled monolithic four-point probe system (probe spacing = 8 or 10 μm) [5]. The four-point-probe resistance R was measured from the slope of linear current-voltage curves that were obtained by sweeping the current I flowing between the outer pair of probes and measuring the voltage drop V between the inner pair of probes, $R = dV/dI$. The ARPES experiments were done in a separate chamber with unpolarized He $I\alpha$ radiation and an electron spectrometer (Scienta SES-100) [7]. The sample temperature was monitored by AuFe-Chromel thermocouples attached close to the sample on the sample holder. First, a clean $Si(111)7 \times 7$ surface was prepared on an n-type or a p-type Si(111) wafer by a cycle of resistive heat treatments. The $Si(111)\sqrt{3} \times \sqrt{3}$-Ag surface superstructure was made by monolayer (ML, 1 ML = 7.8×10^{14} atoms/cm^2) Ag deposition at substrate temperature of $\sim 550\,^{\circ}$C, monitored *in situ* by reflection high-energy electron diffraction (RHEED) [7–9].

Figure 1 presents probe spacing (d) dependence of four-point-probe resistance R of the $\sqrt{3} \times \sqrt{3}$-Ag taken at RT with the four-tip STM prober [6]. The resistance on a
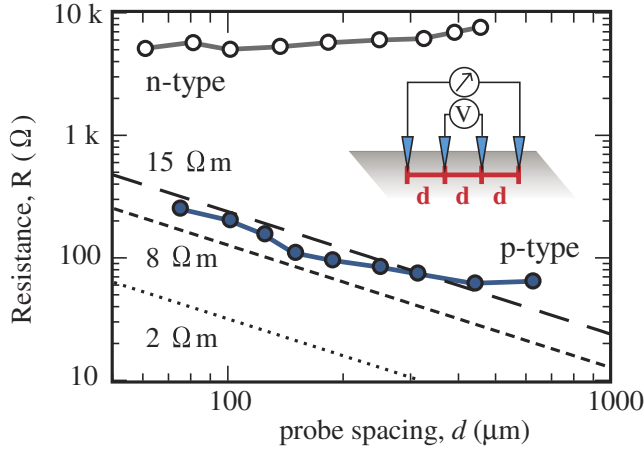
FIG. 1 (color online). Probe-spacing (d) dependence of the resistance of Si(111)$\sqrt{3} \times \sqrt{3}$-Ag measured at RT for wafers having resistivity of 2–15 Ω cm n-type (open circle) and 8–15 Ω cm p-type (solid circle). The dependence of 3D bulk Si with selected resistivity are shown as broken lines. Schematic drawing of the MFPP method is also given.

p-type Si wafer is inversely proportional to d while that of the n-type wafer is almost independent of d. From Ohm's law, the four-point-probe resistance of homogeneous semi-infinite 3D samples has d^{-1} dependence while that of infinite 2D samples is independent of d [6]. Near the surface region, there exist three channels of conduction, a surface-state layer, a space-charge layer, and a bulk layer. The d^{-1} dependence of measured resistance for the p type means that it originates mainly from the bulk Si substrate [6]. On the other hand, the resistance of the n type corresponds to electron transport only through the surface-state and space-charge layers, because it shows 2D character. This distinction between n- and p-type substrates is due to a pn junction [4,6] formed between the surface space-charge layer (inversion layer) and underlying bulk only for n-type substrates. Because of this higher surface sensitivity, further transport experiments were done on the n-type wafers.

Figure 2(a) shows temperature dependence of resistance with various Ag coverage. With increase of Ag coverage and completion of the $\sqrt{3} \times \sqrt{3}$-Ag phase from the 7×7 phase, the resistance at RT decreases. Furthermore, the temperature dependence below RT changes with Ag coverage; the measured resistance becomes higher by cooling for the 7×7 clean surface [12,13], while it becomes smaller for the $\sqrt{3} \times \sqrt{3}$-Ag.

The sheet conductivity, $\sigma_{2D} = (\ln 2/\pi)R^{-1}$, around 1 ML coverages is plotted in Fig. 2(b). Temperature coefficient of σ_{2D}, $\partial \sigma_{2D}/\partial T$, is negative around RT but it becomes positive around 150 K at 1 ML and the inversion transition likely occurs at the higher temperature when the $\sqrt{3} \times \sqrt{3}$-Ag is prepared not at the optimal Ag coverage. As described in Fig. 1, the σ_{2D} values have two contributions from a surface-state layer (its conductivity = σ_{SS}) and a space-charge layer (σ_{SC}); $\sigma_{2D} = \sigma_{SS} + \sigma_{SC}$. The
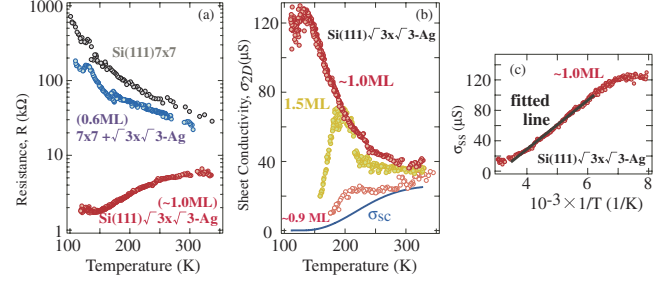
FIG. 2 (color online). (a) Temperature-dependent electrical resistance of a Si(111) surface with various Ag coverages. The structures observed by RHEED are indicated. (b) Sheet conductivity σ_{2D} of Si(111)$\sqrt{3} \times \sqrt{3}$-Ag with various Ag coverages. The simulation of the space-charge-layer conductivity σ_{SC} is also shown. (c) Surface-state conductivity, σ_{SS}, of Si(111)$\sqrt{3} \times \sqrt{3}$-Ag (1 ML) as a function of $1/T$.

σ_{SC} estimated for the present inversion layer based on the Poisson equation [4,14], is also depicted in Fig. 2(b). It is noted that σ_{SS} and σ_{SC} involve electrons and holes as carriers, respectively. According to the previous photo-emission experiments, energy difference between the bulk valence band maximum (E_{VBM}) and the Fermi level (E_F) has been reported to be 0.1–0.2 eV [7,15]. The σ_{SC} in Fig. 2 is an estimation with $E_F - E_{VBM} = 0.13$ eV. The σ_{SC} is frozen out below 150 K. Such dependence is opposite to the experimental data with 1.0 ML Ag coverage. Therefore, the measured conductivity originates mainly from the surface-state layer and the changes with respect to temperature and coverage are deliberated below.

Let us first discuss transport mechanisms in temperature region where $\partial \sigma_{2D}/\partial T$ is negative. Since the surface state is an isotropic 2D metal, the σ_{SS} term is expressed by the Boltzmann picture [7] as $\sigma_{SS} = \frac{e^2}{2} l v_F \mathcal{D}^{2D}$, where v_F is the Fermi velocity and $\mathcal{D}^{2D}$ is the density of states at E_F. l is mean free path, given by $l = \tau v_F$, where τ is relaxation time. In the temperature range of 100–300 K, the e-ph interaction generally dominates electrical conduction for typical metals [16]. Therefore, τ is given by $\tau \sim \tau_{e\text{-ph}} = \hbar/2\pi\lambda_{tr}k_B T$ at high temperature limit ($T > T_D/3$) [17,18]. Since the surface Debye temperature T_D is 140 K as reported by the positron diffraction experiment [19], the present formula is appropriate. A dimensionless constant, λ_{tr}, represents the strength of the e-ph interaction and it is called the coupling parameter or the mass-enhancement factor [17]. From these arguments σ_{SS} should increase linearly with $1/T$, which is exactly found in Fig. 2(c). From the slope of fitted line of σ_{SS} and the band parameters [7,8], we found $\lambda_{tr} = 0.8 \pm 0.5$. It is emphasized that the large uncertainty is not due to the conductivity measurements but due to uncertainty in $v_F = \frac{\hbar k_F}{m*}$ or k_F value that varies from sample to sample ($k_F = 0.05$–0.1 Å^{-1}) [7–9].

The e-ph coupling constant λ can also be determined from temperature-dependent ARPES measurements as has been done for various crystalline metal surfaces [17,20].

We have independently performed such measurements on the $\sqrt{3} \times \sqrt{3}$-Ag surface. Energy width of the surface-state photoemission peak is equal to $\hbar/\tau_{hole}$, where τ_{hole} is lifetime of the surface-state hole excitation. At high temperature limit, the temperature dependence of τ_{hole} is due to the phonon contribution [18,20], given by $\hbar/\tau_{hole} = 2\pi\lambda k_B T$. Therefore, λ is easily measured from a slope of photoemission peak width vs temperature curve.

A measured dispersion curve of the metallic surface-state band of $\sqrt{3} \times \sqrt{3}$-Ag is shown in Fig. 3(a). We chose an energy distribution curve (EDC) at $k_{\parallel} = 0$ to analyze the temperature dependence. The selected spectra are shown in Fig. 3(b), obviously indicating smaller peak width at lower temperature. To extract the energy width, an EDC is fitted by a Gaussian-convoluted Lorentzian with a background of Fermi-Dirac function [18,21]. The Gaussian width is responsible for an actual instrumental resolution and it is fixed at 35 meV. The energy width monotonically increases with temperature for surfaces of both $k_F = 0.05$ and 0.08 Å^{-1} in Fig. 3(c). By fitting the energy widths at various temperatures with a straight line, the slope gives $\lambda = 0.43 \pm 0.03$. We have also found $\lambda = 0.4 \pm 0.1$ for temperature dependence of momentum width (FWHM) of a momentum distribution curves (MDC) at E_F, Fig. 3(c), by the analysis described in Ref. [22]. The λ thus obtained is in a range of those determined from surface conductivity measurements.

As a result, the surface-state conductivity, σ_{SS}, of $\sqrt{3} \times \sqrt{3}$-Ag at 300–150 K is governed mainly by the surface
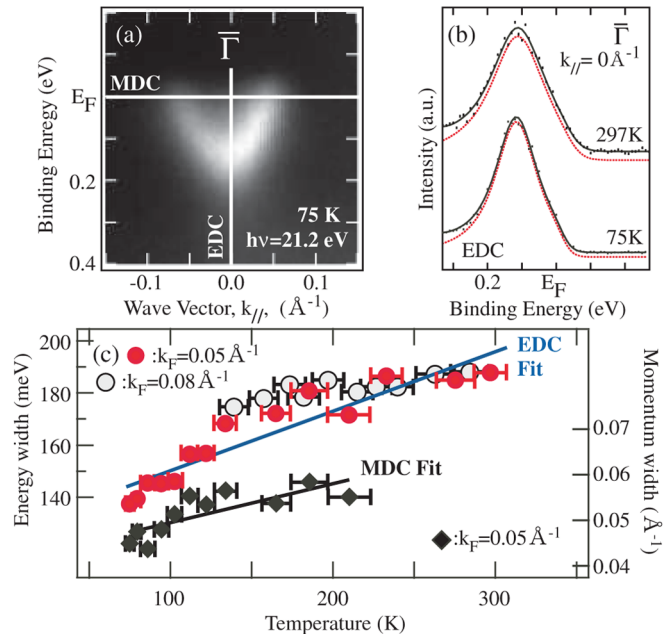
FIG. 3 (color online).   (a) A photoemission band dispersion diagram of Si(111)$\sqrt{3} \times \sqrt{3}$-Ag at $\bar{\Gamma}$ point. (b) Energy distribution curves with the fitted (red) and Gaussian-convoluted Lorentzian (black) curves. (c) Energy and momentum widths vs temperature for the surface of $k_F = 0.05$ ($\sim$1 ML) and 0.08 ($\sim$1.5 ML) Å^{-1} with fitted lines.

e-ph interaction. It is noted that the value of $\lambda \sim 0.4$ is larger than those of Ag(111) clean surface [20] ($\lambda = 0.12$) and bulk Ag crystal [20] ($\lambda = 0.15$), but smaller than that of the Si(111)7×7 clean surface [21] ($\lambda = 1.06$). The $\sqrt{3} \times \sqrt{3}$-Ag surface is likely classified as a weak e-ph interacting system [16]. Adopting the parameter of $\lambda_{tr} = \lambda \sim 0.4$, carrier relaxation time is estimated to be 1.0×10^{-14} s at 300 K (3.1×10^{-14} s at 100 K), which is the same order of magnitude as that for bulk Ag crystal [16], 4.0×10^{-14} s at 273 K. Then, the carrier mean free path is 45–90 Å at 300 K (140–270 Å at 100 K) for $k_F = 0.05$–0.1 Å^{-1}. The mean free path is 1 order of magnitude shorter than that in bulk Ag crystal ($\sim$560 Å at RT) [16].

Finally, we consider the temperature region below $\sim$150 K, where $\partial\sigma_{2D}/\partial T$ is positive in Fig. 2. Such a phenomenon cannot be explained by the conventional metallic conduction. However, insulating transports of 2D metal layers have been known in Si-MOSFET [23] and GaAs-AlGaAs heterostructures [24]. The origins have been proposed possibly to be the electron-electron interactions by disorder potentials in samples but the arguments have not been settled yet. A new 2D metal system of the Si(111)$\sqrt{3} \times \sqrt{3}$-Ag surface is expected to provide a different point of view for the issue.

As found in Fig. 2, drastic decreases of the surface conductivity at lower temperatures are likely reinforced when the Ag coverage is not optimum for the $\sqrt{3} \times \sqrt{3}$-Ag surface. On the other hand, no energy gap-opening at E_F was found for the surface-state band from ARPES from RT to 75 K (Fig. 3), indicating no relation to formation of a band insulator. It has also been known that Si(111)$\sqrt{3} \times \sqrt{3}$-Ag exhibits a phase transition of symmetry breakdown in the atomic structure [25] and the transition temperature is similar to which the measured conductivity starts to decrease drastically (Fig. 2). According to the recent structural researches [19,26], the transition is an order-disorder type and, therefore, the surface-state conductivity should increase by cooling through the transition due to suppression of the structural fluctuations. It looks, therefore, that there is no direct relation to the conductivity either. As a consequence, the phenomenon seems to be related to localization of electron wave function due to interactions between electrons and defects, which are enhanced at low temperature.

Carrier scattering at a point defect in metal crystal is generally elastic and only contributes to the residual resistance [16]. On the other hand, in a 2D surface atomic layer, there are 1D line defects such as atomic steps and domain boundaries (Fig. 4), which are inevitable scatterers for surface-state electrons [3]. Furthermore, a Friedel oscillation, an oscillatory modulation of electrostatic potential, occurs around every surface defect through coherent interference of electron waves due to suppression of e-ph interaction at low temperature and it has been directly observed on the present surface by STM [3,10,11]. Therefore, we speculate that the decrease of surface-state
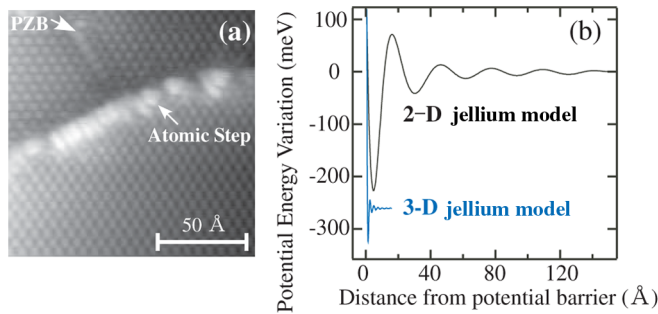
FIG. 4 (color online). (a) A STM image of 1D line defects, out-of-phase domain boundary (PZB) and an atomic step, on the $\sqrt{3} \times \sqrt{3}$-Ag observed at 65 K. (b) Density functional calculations of potential energy variation for 2D (3D) jellium model as a function of distance from a 1D (2D) potential barrier. The band parameters are given in the text.

conductivity below $\sim$150 K is due to such random potential modulations around defects. It is to note that such a localization effect are likely enhanced due to formation of additional domain boundaries (twin boundaries [25]) through the transition of symmetry breakdown. Furthermore, Friedel oscillations also grow drastically at the phase transition since the coherence length of surface-state electrons is elongated by suppression of the dynamical disorders. From the data with below and above the optimal $\sqrt{3} \times \sqrt{3}$ Ag coverage in Fig. 2(b), the temperature where the sign of $\partial \sigma_{2D}/\partial T$ changes, increases to ca. 200 K. This may be due to presence of residual imperfect domains (7×7 and 6×1-Ag) and excess Ag adatoms on top of the $\sqrt{3} \times \sqrt{3}$-Ag surface [27], which also contribute to create the Friedel oscillations around them.

To demonstrate the effect, we have performed density functional calculations [28] with the jellium model. We focus on electron-potential modulation of 2D electron gas scattered at a 1D potential barrier representing surface defects of atomic steps and domain boundaries, with the present band parameters, $k_F = 0.1$ Å^{-1}, $m^*/m_0 = 0.1$, and a monatomic layer thickness of 3 Å. For a comparison, we have also calculated for a 3D electron gas with a 2D potential wall, representing a grain boundary in a 3D crystal grain, with band parameters of typical bulk metal, $r_s/a_0 = 3$ and $m^*/m_0 = 1$ [16]. As shown in Fig. 4, the modulation of the present 2D system have much larger potential amplitude and longer effective decay length than that in the 3D bulk system, due to difference in the dimensionality and electron density. Therefore, through overlaps of these modulations formed from every surface line and point defects, additional random potentials appear on the surface [10]. And, by sufficient enhancement of the potential amplitude at low temperature, it can cause strong (Anderson) localization. Especially, since the periodicity of oscillatory modulation in potential is about π/k_F, which is a half of the Fermi wavelength, the Fermi electrons are effectively reflected by the potential modulation. Because

of complexity of electron-defect interactions, the present scenario only provides one possible aspect. Further researches on electron transports in various surface atomic layers are requested for complete understanding of this localization.

In summary, through transport experiments with MFPP and electronic-state analysis by ARPES, we found that the surface-state conductivity of Si(111)$\sqrt{3} \times \sqrt{3}$-Ag was governed by electron-phonon interaction from RT to $\sim$150 K, while by the strong electron localization below it. We speculate that this behavior is related to random potential variation caused by Friedel oscillation of surface electrons around defects.

*imatsuda@issp.u-tokyo.ac.jp
[1] D. K. Ferry and S. M. Goodnick, *Transport in Nano-structures* (Cambridge University Press, Cambridge, England, 1997).
[2] *Anderson Localization*, edited by Y. Nagaoka and F. Fukuyama (Springer, New York, 1982).
[3] I. Matsuda *et al.*, Phys. Rev. Lett. **93**, 236801 (2004).
[4] T. Tanikawa *et al.*, Phys. Rev. Lett. **93**, 016801 (2004).
[5] T. Tanikawa *et al.*, e-J. Surf. Sci. Nanotech. **1**, 50 (2003).
[6] S. Hasegawa *et al.*, Surf. Rev. Lett. **10**, 963 (2003).
[7] I. Matsuda *et al.*, Phys. Rev. B **71**, 235315 (2005).
[8] T. Hirahara *et al.*, Surf. Sci. **563**, 191 (2004).
[9] J. N. Crain *et al.*, Phys. Rev. B **66**, 205302 (2002).
[10] M. Ono *et al.*, Phys. Rev. Lett. **96**, 016801 (2006).
[11] N. Sato *et al.*, Phys. Rev. B **59**, 2035 (1999).
[12] T. Tanikawa *et al.*, Phys. Rev. B **68**, 113303 (2003).
[13] J. W. Wells *et al.*, Phys. Rev. Lett. **97**, 206803 (2006).
[14] A. Many, Y. Goldstein, and N. B. Grover, *Semiconductor Surfaces* (North-Holland, Amsterdam, 1965), Chap. 4.
[15] X. Tong, S. Hasegawa, and S. Ino, Phys. Rev. B **55**, 1310 (1997).
[16] N. W. Ashcroft and N. D. Mermin, *Solid State Physics* (Thomson Learning, London, 1976).
[17] G. D. Mahan, *Many-Particle Physics* (Kluwer Academic/Plenum, New York, 2000), Chap. 8.
[18] T. Balasubramanian *et al.*, Phys. Rev. B **57**, R6866 (1998).
[19] Y. Fukaya, A. Kawasuso, and A. Ichimiya, e-J. Surf. Sci. Nanotech. **3**, 228 (2005).
[20] E. W. Plummer *et al.*, Prog. Surf. Sci. **74**, 251 (2003).
[21] I. Barke *et al.*, Phys. Rev. Lett. **96**, 216801 (2006).
[22] J. E. Gayone *et al.*, Appl. Phys. A **80**, 943 (2005).
[23] S. V. Kravchenko *et al.*, Phys. Rev. B **51**, 7038 (1995).
[24] E. Ribeiro *et al.*, Phys. Rev. Lett. **82**, 996 (1999).
[25] N. Sato, T. Nagao, and S. Hasegawa, Surf. Sci. **442**, 65 (1999).
[26] K. Sakamoto *et al.*, Phys. Rev. B **73**, 193303 (2006).
[27] N. Sato, T. Nagao, and S. Hasegawa, Phys. Rev. B **60**, 16 083 (1999).
[28] A. Liebsch, *Electronic Excitation at Metal Surfaces* (Plenum, New York, 1997), Chap. 2.